Available online at www.sciencedirect.com
SCIENCE DIRECT®

Journal of the European Ceramic Society 23 (2003) 2435–2441
www.elsevier.com/locate/jeurceramsoc

Structure–property relations in xCaTiO$_3$–(1−x)SrMg$_{1/3}$Nb$_{2/3}$O$_3$ based microwave dielectrics

H. Bagshaw[a,*], D. Iddles[b], R. Quimby[a], I.M. Reaney[a]

[a]University of Sheffield, Department of Engineering Materials, Sir Robert Hadfield Building, Mappin Street, Sheffield S1 3JD, UK
[b]Filtronic Comtek, Ceramics Division, Enterprise Drive, Four Ashes, Wolverhampton WV10 7DB, UK

Abstract

Solid solutions of the system (x)CaTiO$_3$–(1−x)Sr(Mg$_{1/3}$Nb$_{2/3}$)O$_3$ (CTSMN) were prepared by the mixed oxide route. All compositions were found to be single phase by X-ray diffraction; pellets had densities >95% of the theoretical X-ray density. Scanning electron microscopy coupled with energy dispersive X-ray analysis revealed a homogeneous distribution of cations within instrument sensitivity in all samples except for pure SMN which showed evidence of some unreacted MgO. SMN is reported as a 1:2 ordered trigonal/hexagonal complex perovskite structure in the X-ray data files but electron diffraction revealed superlattice reflections characteristic of both in-phase and anti-phase rotations of octahedra arising from further structural phase transitions on cooling. These reflections were retained throughout the solid solution range but $\pm 1/3\{hkl\}$ ordered superlattice reflections were absent in samples where $x > 0.1$. In general, the microwave quality factor (Q_u*f_o) decreased as x increased and the temperature coefficient of resonant frequency (TCf) was approximately linearly proportional to the permittivity; at $x \sim 0.20$: TCf$\sim$0, $\varepsilon_r \sim 45$ and Q_u*$f_o \sim 9000$.

Keywords: Perovskites; Microwave ceramics; Solid solutions; Electron microscopy; X-ray methods; CaTiO$_3$; Sr(Mg,Nb)O$_3$

1. Introduction

CaTiO$_3$ (CT) is a good candidate for a microwave dielectric since it has a high dielectric constant ($\varepsilon_r = 160$) and unloaded quality factor ($Q_u = 8000$ at 1.5G Hz) but unfortunately it has a large positive temperature coefficient of resonant frequency (TCf = +850 MK^{-1}).[7] In order to produce a zero TCf material, one may form a solid solution combining CaTiO$_3$ with a material exhibiting a negative TCf. Sr(Mg$_{1/3}$Nb$_{2/3}$)O$_3$ (SMN) has been reported as having a small negative TCf (−14 MK^{-1}), $\varepsilon_r = 33$ and $Q_u = 20{,}000$ at 3 GHz) and is therefore a good candidate compound.[7]

Sr-based perovskites of general formula Sr(B′$_{1/3}$B″$_{2/3}$)O$_3$ often show stoichiometric cation ordering on the B site. The ordered lattice involves the stacking of one layer of B′ species (i.e. Mg in this instance) followed by two layers of B″(Nb) on the B site {111} planes. This gives rise to a superstructure which has hexagonal symmetry, isostructural with Ba(Sr$_{1/3}$Ta$_{2/3}$)O$_3$..[2,3] This effect produces superlattice reflections at $\{h \pm 1/3, k \pm 1/3, l \pm 1/3\}$. 1:2 ordering of the B site cations is also evidenced by splitting or broadening of the major perovskite peaks.[2,3]

CT on the other hand is a simple perovskite which undergoes a series of high temperature phase transitions involving rotations of the octahedra to give an orthorhombic structure at room temperature. The octahedral tilt transitions give rise to superlattice reflections which lie at $\frac{1}{2}hkl_p$ and $\frac{1}{2}hk0_p$ reflections (where 'p' denotes a pseudocubic setting) in diffraction patterns arising from anti-phase and in-phase rotations of the oxygen-octahedra respectively.[4,5] In addition, the Ca ions displace in an antiparallel configuration, resulting in the appearance of $\frac{1}{2}\{h00\}_p$ reflections.[4,5]

This paper investigates the changes in symmetry which occur across the (x)CaTiO$_3$–(1−x)SrMg$_{1/3}$Nb$_{2/3}$O$_3$ (CTSMN) solid solution and relates the structural changes to microwave dielectric properties.

2. Experimental

2.1. Ceramic processing

Solid solutions of the system (x)CaTiO$_3$–(1−x)Sr(Mg$_{1/3}$Nb$_{2/3}$)O$_3$ were prepared by the mixed oxide route. Starting materials (>99.9% pure and supplied by Filtronic Comtek) were mixed in the

* Corresponding author.

0955-2219/03/$ - see front matter © 2003 Elsevier Ltd. All rights reserved.
doi:10.1016/S0955-2219(03)00132-8

appropriate ratios and milled for 16 h in polypropylene pot using Y-stabilised ZrO_2 media. Batches were then calcined in an Al_2O_3 crucible between 1150 and 1250 °C depending on composition. The calcined powders were sieved and re-milled under the same conditions as above down to a particle size of ~2 μm (Laser Coulter analysis). After drying, a binder was added to the powder and remilled for 1h. The powder was then pressed as 1 or 2 cm pellets using a uniaxial press under a pressure of ~200 MPa. The green pellets were then placed on a calcia-stabilised zirconia board and sintered in air at 1600 °C.

2.2. X-ray diffraction (XRD)

The calcined powders were examined using a Phillips PW1730/10 diffractometer operated at 50 kV and 30 mA. Scans were run with Cu$K_{\alpha 1}$ radiation ($\lambda = 0.1540562$ nm) over the range 10–90° 2θ with a step size of 0.02 and a scan rate of 2/min. Data analysis was performed with Sietronics XRD Trace Processing Software (version 2.0) and STOE WinXPOW software.

2.3. Scanning electron microscopy (SEM)

Samples were polished until flat with a mirror finish and then thermally etched at 100 °C below the sintering temperature for 1 h using the same heating and cooling rates as sintering (4 °C/min). The samples were mounted on stainless steel stubs using silver dag and carbon coated. Samples were examined using a CAMSCAN SEM operating at 15 kV. Images were obtained in secondary electron mode. The SEM was equipped with a LINK energy dispersive X-ray (EDS) detector and ancillary electronics.

2.4. Transmission electron microscopy

Samples were mounted on a glass slide using a thermosensitive resin and ground to approximately 20 μm thick after which a 3.05 mm Cu support ring with 800 μm circular hole was glued onto its surface using an epoxy resin. The sample was removed from the glass slide and excess thermosensitive resin removed using acetone. The samples were thinned in a Gatan Duo Mill ion beam thinner operating at an accelerating voltage of 6 kV and a combined gun current of 0.6 mA at an incidence angle of 15°. The samples were examined using an EM420 TEM operating at an accelerating voltage of 120 kV.

2.5. Microwave dielectric measurements

Microwave measurements (ε_r, Q and TCf) were performed using a silver plated aluminium cavity > ~4 times the diameter of the test resonator, (this ensured an "isolated" but shielded resonator) and an Agilent vector network analyser (8753ES) with a range from 30 kHz–6 GHz. Sintered samples were located at the centre of the cavity on a 99.5% alumina support, thus avoiding any influence from the metallic cavity walls. Microwave energy was coupled to the test piece using a single probe, measuring in reflectance. After calibration for the cables and cavity, the coupling was adjusted such that losses were lower than −30 dB. Q is approximated using Eq. (1):

$$Q = f_0/\mathrm{BW} \quad (1)$$

Where f_o is the resonant frequency and BW is the bandwidth measured at 7 dB from the resonant peak minimum. Measurement of Q was at ambient temperature and the resonance mode measured was $TE_{01\delta}$. TCf measurements were performed in the same aluminium cavity placed inside a Tenney temperature control cabinet. Resonant frequency measurements were performed at 60, 20 and −10 °C when the $TE_{01\delta}$ mode was stable. τ_f was calculated using Eq. (2):

$$\mathrm{TCf} = (f_{60} - f_{-10})/(f_{20} \times 70) \quad (2)$$

where f_{60} is the resonant frequency at 60 °C, f_{-10} is the resonant frequency at −10 °C and f_{20} is the resonant frequency at 20 °C.

3. Results and discussion

Fig. 1 shows XRD traces for $(x)CaTiO_3$–$(1-x)SrMg_{1/3}Nb_{2/3}O_3$ compositions with various values of x. All compositions could be indexed according to either JCPDS card 78-1013 (CT) or 17-181 (SMN). No peaks associated with any secondary phases were observed. Both end members showed sharp discrete peaks whereas the intermediate compositions in the series (particularly CTSMN, $x = 0.25$–0.75) exhibited peak broadening. The peaks were displaced to lower 2θ angles with increasing SMN content, which is consistent with substitution of the larger Sr ion for Ca on the A site and larger Mg and Nb, for Ti onto the B site. Traces are overlaid (Fig. 1) to illustrate changes in peak intensity and position across the series.

Fig. 2a–c show SEM images of CT, SMN and CTSMN ($x = 0.5$), respectively. CT shows a grain size distribution around ~5 μm with little porosity, consistent with measured densities >95% of the theoretical X-ray density. No secondary phases are observed. SMN also shows an even grain size distribution (~5 μm) with little porosity, in agreement with measured densities (>95%); however, white flecks were present on the surface. Further analysis using EDS revealed that they were rich in Mg and it was concluded that they were unreacted MgO. For CTSMN ($x = 0.5$) (Fig. 2c), the grain size distribution is not as homogeneous as for $CaTiO_3$ and SMN but little porosity is observed.

Fig. 3a and b are bright field TEM images from grains in a sample of (a) CT showing a typical ferroelastic

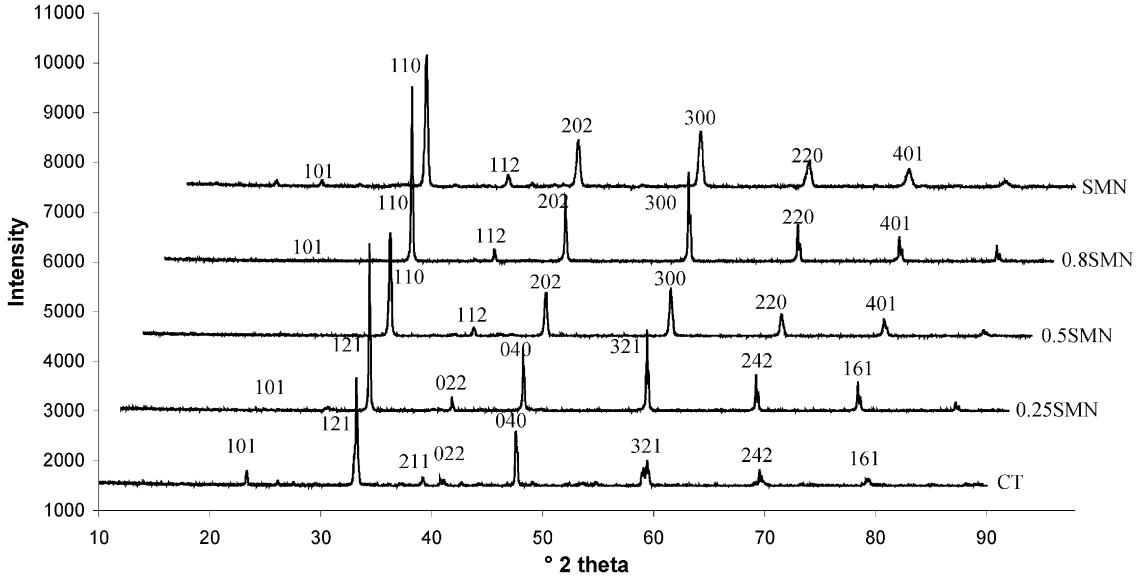

Fig. 1. XRD traces for the CT-SMN solid solution series. CT and 0.25SMN traces indexed according to $CaTiO_3$ (JCPDS card 78-1013), 0.5SMN to SMN traces indexed according to $Sr(Mg_{1/3}Nb_{2/3})O_3$) JCPDS card 17-181).

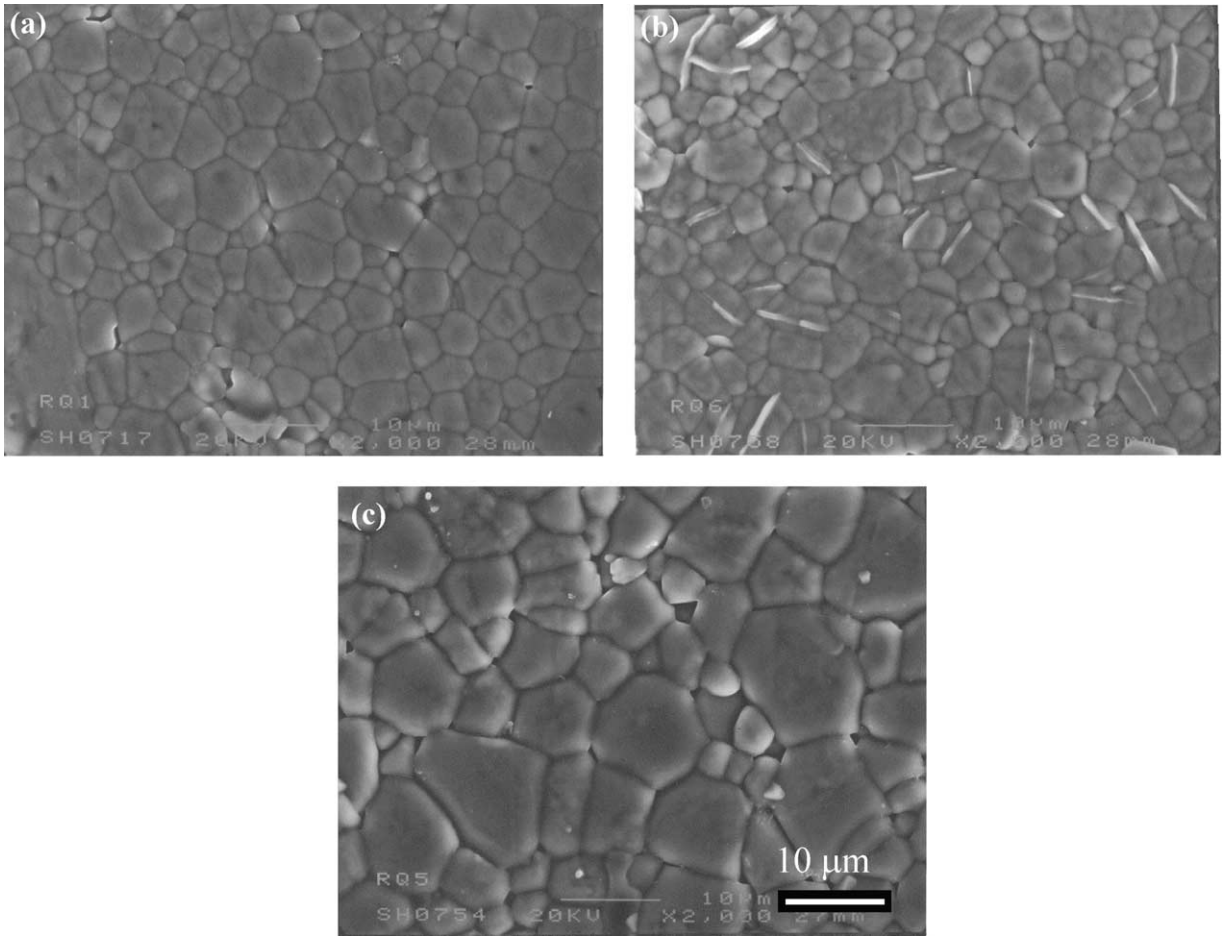

Fig. 2. SEM images of thermally etched (a) CT, (b) SMN and (c) CTSMN ($x = 0.5$).

domain structure, and (b) CTSMN ($x=0.5$). Similar domains to that shown in Fig. 3a are observed in all compositions indicating that the solid solution is structurally distorted for all values of x. Fig. 4 a–d are zone axis diffraction patterns (ZADPs) for (a) CT, (b) SMN and (c and d) CTSMN $x=0.5$. Fig. 4a is a<111> ZADP and the strong reflections may be indexed according to a simple perovskite structure. However, weaker, superlattice reflections are present at $\frac{1}{2}\{hk0\}$ positions. According to Glazer,[8] CT has an $a^-a^-c^+$ tilt system which gives rise to an orthorhombic unit cell at room temperature (Pbnm). The notation denotes that

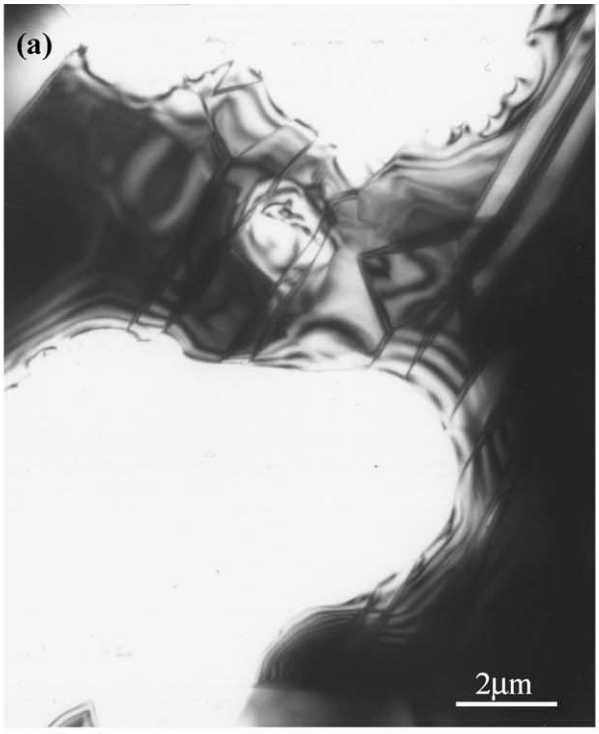

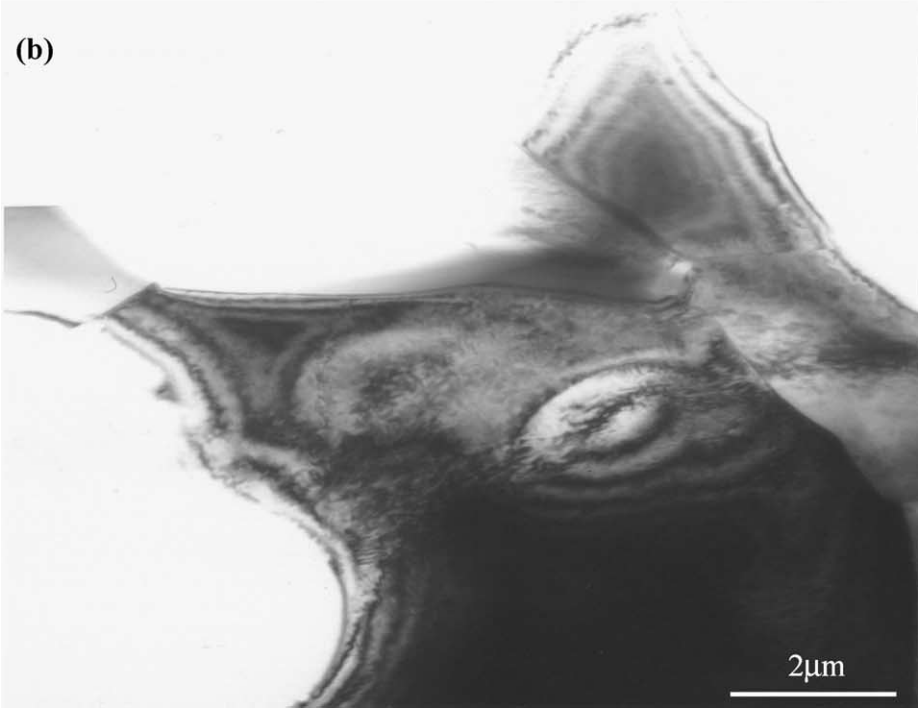

Fig. 3. Bright field TEM image of a typical (a) CT and (b) CTSMN ($x=0.5$).

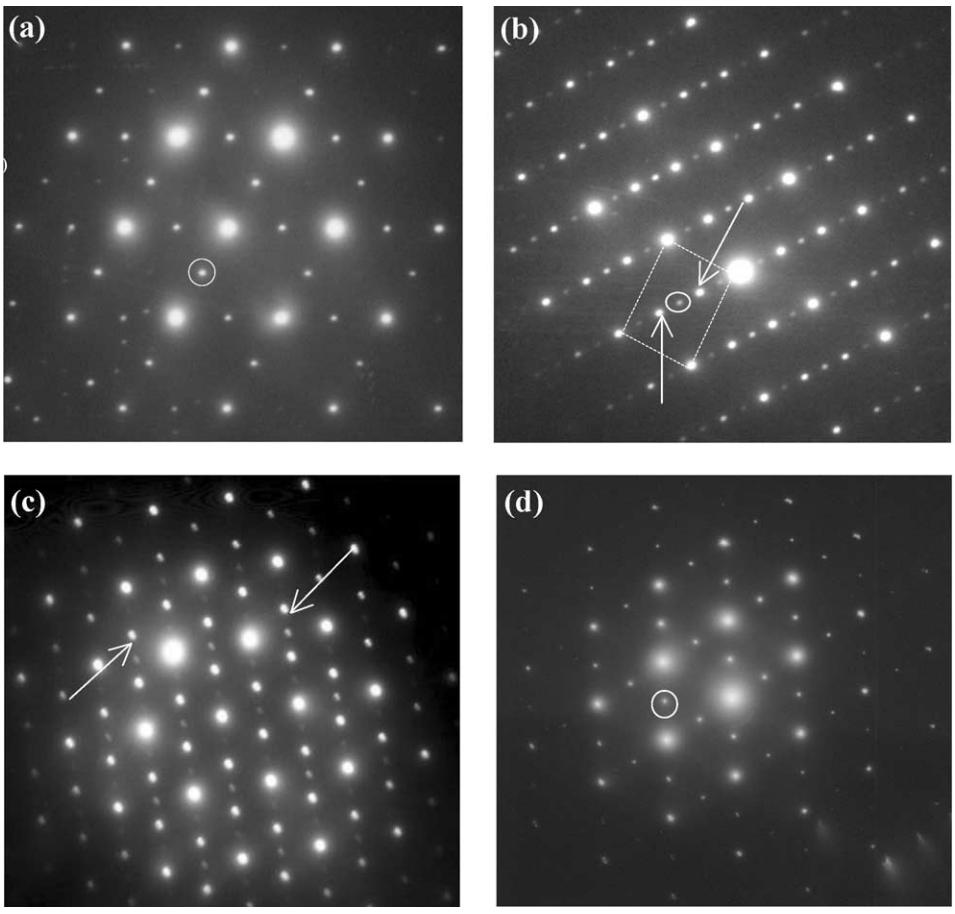

Fig. 4. Electron diffraction patterns from (a) CT–<111> ZADP with $\frac{1}{2}\{hk0\}$ in phase tilt reflection circled, (b) SMN–<110> ZADP with the fundamental reflections highlighted by the dotted rectangle, $1/3\{hkl\}$ 1:2 ordered reflections arrowed and, $\frac{1}{2}\{hkl$ antiphase tilt reflections circled, (c) <110> ZADP from CTSMN ($x=0.5$) with $\frac{1}{2}\{hkl\}$ antiphase tilt reflections (weakest reflections are $\frac{1}{2}\{h00\}$ from antiparallel cation displacements), (d) <111> ZADP from CTSMN ($x=0.5$) with $\frac{1}{2}\{hk0)$ in phase tilt reflections circled.

two of the orthogonal axes are tilted in anti-phase and the third in-phase. The latter mode of tilting gives rise to odd–odd–even (ooe) reflections at half integer positions, e.g. $\frac{1}{2}\{310\}$ $\frac{1}{2}\{312\}$. The latter reflections are allowed by the zone law in $<111>_p$ ZADP's confirming that CT is tilted-in phase. However, the same reflections were observed in $<111>_p$ ZADP's from all compositions (e.g. Fig. 4d), implying that all CTSMN compounds are

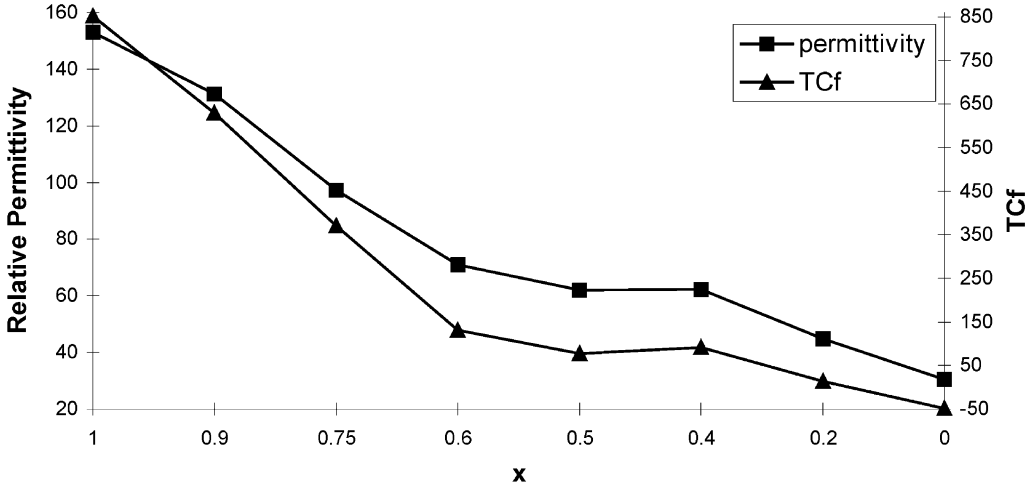

Fig. 5. ϵ_r and TCf as a function of composition (x) for the CTSMN solid solution series.

tilted in-phase, including SMN. Fig. 4b is a<110>p ZADP from SMN in which superlattice reflections are observed at $\frac{1}{3}\{hkl\}$ in addition to $\frac{1}{2}\{hkl\}$ positions. The former confirms that the B-site sublattice is ordered in a 1:2 Mg:Nb ratio as expected for SMN.[4] These reflections are absent for samples where $x > 0.1$. The $\frac{1}{2}\{hkl\}$ reflections are consistent with the presence of antiphase rotations of the oxygen octahedra and are also present in all compositions. Fig. 4c is a<110> ZADP from CTSMN $x=0.5$. In addition to $\frac{1}{2}\{hkl\}$ superlattice reflections, $\frac{1}{2}\{h00\}$ reflections are present. According to Glazer[8] and Reaney et al.,[4] these reflections are associated with antiparallel A-site cation displacements.

From the above data, it is clear that SMN is not simply an ordered complex perovskite but it is also structurally distorted at room temperature as a result of rotations of oxygen-octahedra on cooling from the sintering temperature. The presence of $\frac{1}{2}\{hk0\}$ and $\frac{1}{2}\{hkl\}$ reflections imply a tilt system which contains both antiphase and in-phase octahedral rotations, consistent with an $a^-a^-c^+$ configuration. This tilt configuration is identical to that refined for CT.[8] It is concluded therefore that the room temperature structure of CTSMN is tilted across the entire series with only the appearance of 1:2 B-site ordering ($x<0.1$), distinguishing, in terms of symmetry, between values of x.

3.1. Electrical properties

Fig. 5 is a plot of relative permittivity (ε_r) and TCf as a function of composition (x) for CTSMN. Both TCf and ε_r increase with x. At approximately $x=0.2$, TCf 0 and $\varepsilon_r=45$. Fig. 6 is a plot of ε_r as a function of TCf for the same samples. TCf is approximately linearly proportional to ε_r therefore suggesting that tuning of TCf in this system can be attributed mainly to dilution of permitivitty.[6] Fig. 7 is a plot of $Q_u{*}f_0$ values as a function of

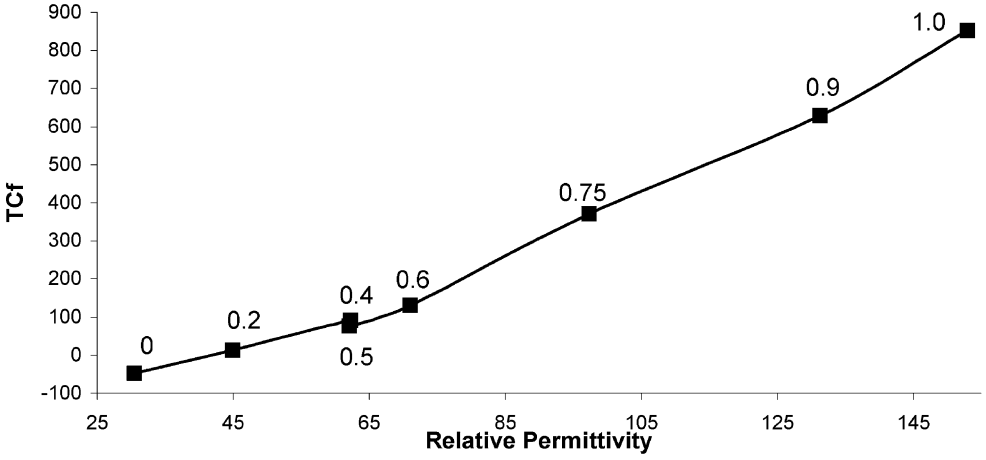

Fig. 6. TCf as a function of ε_r for the CTSMN solid solution series. Value of x is indicated for each composition.

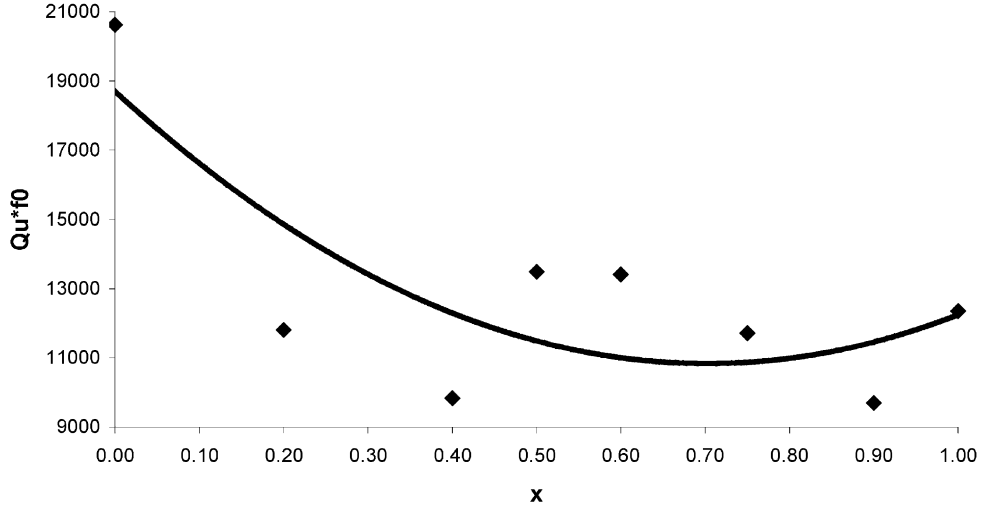

Fig. 7. $Q_u{*}f_0$ as a function of composition (x) for the CTSMN solid solution series.

x. $Q_u{*}f_0$ is a maximum (21,000) for the ordered SMN composition and decreases to 9000 for $x=0.4$ before increasing to 12,000 for CT. Although TCf of CTSMN tunes through zero with a permittivity equivalent to CTNA (45), the $Q_u{*}f_0$ values are poor (9000). The question remains as to why this should be the case. The compounds are single-phase perovskites and the pellets were dense thus suggesting the low Q value is not associated with inner impurity phases or porosity. The permittivities are comparable to CTNA, have similar average tolerance factors and identical crystal symmetry. These measurements highlight how little is known about the relationship between crystal chemistry and Q. A Raman spectroscopy study of these compounds is presented elsewhere in these proceedings.[9]

4. Conclusions

1. SMN is not only ordered on the B-site but also exhibits in-phase and anti-phase tilt reflections consistent with an $a^-a^-c^+$ tilt configuration.
2. All compositions in CTSMN solid solution are tilted with an $a^-a^-c^+$ system and it is only the appearance of ordering for $x<0.1$ that distinguishes the compositions with respect to symmetry.
3. TCf of CTSMN tunes through zero at $x\approx0.2$ with $\varepsilon_r\approx45$. $Q_u{*}f_0$ is poor, however, despite the fact that the compounds are single phase and the ceramics were dense.

Acknowledgements

The authors would like to thank T. Price for the electrical measurements performed at Filtronic Comtek, Wolverhampton. Thanks also go to Ms. D Bussey and the staff at the Sorby Centre for Electron Microscopy for help with the SEM and TEM work.

References

1. Colla, E. L., Reaney, I. M. and Setter, N., Effect of structural changes in complex perovskites on the temperature coefficient of the relative permittivity. *Journal of Applied Physics*, 1993, **75**(5), 3414–3425.
2. Galasso, F. and Pyle, J., *Journal of Physical Chemistry*, 1561, **67**, 1963.
3. Galasso, F., *Structure, Properties and Preparation of Perovskite-Type Compounds. International Series of Monographs in Solid State Physics*. Peragamon, New York, 1969.
4. Reaney, I. M., Colla, E. L. and Setter, N., Dielectric and structural characterisation of Ba and Sr based complex perovskites as a function of tolerance factor. *Japenese Journal of Applied Physics*, 1994, **84**, 3339–3990.
5. Moulson, A. J. and Herbert, J. M., *Electroceramics*. Chapman and Hall, London, 1990.
6. Reaney, I. M. *et al*., On the temperature coefficient of resonant frequency in microwave dielectrics. *Philosophical Magazine A*, 2001, **81**(2), 501–510.
7. Nomura, Shoichiro, Ceramics for microwave dielectric resonator. *Ferroelectrics*, 1983, **49**, 61–70.
8. Glazer, A. M., The classification of tilted octahedra in perovskites. *Acta Crystallographica*, 1972, **B28**, 3384–3392.
9. Zheng, H., Csetede Gydruyfalva, G. D. C., Quimby, R., Bagshaw, H., Ubil, R., Reaney, I. M. and Yarwood, J., Raman spectroscopy of B-site order–disorder in $CaTiO_3$ based microwave ceramics. *J. Eur. Ceram. Soc*. (in press).